Article

Modified Equation of Shear Strength with Respect to Saturation

Wenjing Tian [1],* , Herman Peiffer [1],* , Benny Malengier [2] , Gang Liu [3] and Liangliang Cheng [4]

[1] Department of Civil Engineering, Ghent University, Technologiepark-Zwijnaarde 68, 9052 Gent, Belgium
[2] Department of Materials, Textiles and Chemical Engineering, Ghent University, Technologiepark-Zwijnaarde 70A, 9052 Gent, Belgium; benny.malengier@ugent.be
[3] Department of Hydraulic & Environment Engineering, China Three Gorges University, Daxuelu Avenue 8, Yichang 443002, China; hkliugang@126.com
[4] Group of Dynamics and Vibration, Engineering and Technology Institute Groningen, Faculty of Science and Engineering, University of Groningen, 9713 GZ Groningen, The Netherlands; liangliang.cheng@rug.nl
* Correspondence: wenjing.tian@ugent.be (W.T.); herman.peiffer@ugent.be (H.P.)

Abstract: Unsaturated soil shear strength is a significant topic in geotechnical engineering. The measurement of unsaturated soil properties such as shear strength and matric suction could be costly, hard, time-consuming, and often impractical to obtain. The purpose of this research is to propose a new shear strength model for unsaturated soil and to predict the shear strength by using the degree of saturation directly because the water saturation is easy to obtain. More specifically, this study focused on Bishop's shear strength theory and van Genuchten's soil–water characteristic curve to describe the effect of saturation on shear strength. The new shear strength model was expressed as a function of saturation degree, residual degree of saturation, effective shear strength indices, net normal stress, and five parameters. The performance of the presented model in this paper was verified by fitting it to data obtained by laboratory tests on silty sand including the triaxial shear test and soil–water characteristic curve test. From these two laboratory tests, we obtained the variation in the matric suction and shear strength with the degree of saturation under various dry densities. This proposed model was also validated against the shear strength results of the clayed-silty sand and Ankara clay recorded in the literature. Comparing the result of the shear strength under the variation of one parameter, this model was much more sensitive regarding parameter m, which was related to the material characteristic. The comparison between the predicted values and experimental points was particularly fine and showed the ability of this model to be applied to a wide range of soils.

Keywords: shear strength; unsaturated soil; suction; van Genuchten model; degree of saturation

1. Introduction

Shear strength is regarded as one of the important mechanical properties in the forecast of the stability of slopes, subgrade bearing capacity, and pressure against a soil-retaining structure. Taking slope failure as an example, after reservoir impounding, reservoir water level fluctuation and rainfall infiltration have become main factors that affect slope stability [1–4]. There are several reasons for this phenomenon. First, infiltrated water increases the sliding area's weight and the pore water pressure, leading to slope failure [5,6]. Second, infiltrated water softens the soil's shear strength and leads to slope failure [7–9]. Therefore, shear strength has a significant impact on the analysis of stability for slope in geotechnical engineering [10].

Many theories or empirical equations have been developed to predict or estimate the shear strength of unsaturated soil. Bishop pointed out an effective stress shear strength equation to explain the mechanical behavior of unsaturated soil [11–13]. Later, two independent stress sources including net normal stress $(\sigma - \mu_a)$ and matric suction $(\mu_a - \mu_w)$ were used to interpret the behavior of soil [14]. These two equations claimed by Bishop and Fredlund were of great importance for shear strength in an unsaturated soil area, however,

matric suction $(\mu_a - \mu_w)$, which is difficult to test, was still included in these two models [15,16]. In order to develop an empirical model of shear strength for unsaturated soil, many scholars such as Abramento [17] and Toll [18] have pointed out an empirical model with fitting parameters. Many of these equations also adopted the soil–water retention curve (SWCC) as the controlling parameter to project shear strength [10,19]. Vanapalli [10] showed a procedure to predict the shear strength of an unsaturated soil by using the soil–water characteristic curve and the saturated shear strength parameters. Zhang [20] proposed an effective stress equation that was able to predict the soil strength and deformation behavior. Lu [21] proposed a closed-form equation for effective stress in unsaturated soil that only required two controlling parameters including the inverse of the air entry pressure and the pore size spectrum number. Other scholars have also discussed empirical models that considered the air-entry value [22] or the distinct element method [23]. However, these models focused on the relationship between the shear strength and matric suction rather than directly considering the water content. In addition, experiments for suction are time-consuming and need an expensive and sophisticated laboratory test system [24,25]. This resulted in a limited application of shear strength empirical equations in engineering and scientific areas. Up to now, there has only been a limited practical application of the unsaturated soil shear strength theory in engineering practice. Nonetheless, engineers can measure the degree of saturation with a simple experimental method at each location. As summarized above, for various engineering fields, it is of great importance to propose a simpler method to directly estimate the shear strength of unsaturated soil including saturation.

This research, based on the unsaturated soil shear strength theory proposed by Bishop and van Genuchten's soil–water characteristic curve model, a new multiple parameter shear strength model was developed to describe the influence of saturation. In this model, the matric suction was replaced by the degree of saturation. In the end, the equation was a function of saturation degree, residual saturation degree, effective cohesion, effective angle of internal friction, and net normal stress. The proposed model was validated against experimental points from experiments such as the triaxial shear test and the SWCC test as well as the literature data reported for clayed-silty sand [26] and Ankara clay [27]. Section 2 introduces the development of the new shear strength model. The material and experimental test system described in Section 3 provides the data of the shear strength and matric suction under an increasing degree of saturation, which could support this model. Next, the comparison between the model prediction and the measured data are given in Section 4 to validate and examine the effectiveness of the proposed model. Subsequently, the comparison between model prediction and measured data in the literature is also shown in Section 4. The parameter sensitivity analysis is shown in Section 5 to examine the robustness of the proposed model and evaluate whether the results are affected by varying key parameters.

2. Theory

2.1. Bishop Shear Strength Model

The shear strength of unsaturated soil put forward by Bishop [12] is well-suited to characterize the effect of suction on the unsaturated soil, and has been widely adopted in many geotechnical engineering applications. Bishop extended the definition of soil to unsaturated soil and modified the shear strength equation as follows:

$$\tau_f = c' + (\sigma - u_a)tan\phi' + \chi(u_a - u_w)tan\phi' \tag{1}$$

where τ_f is the shear strength; c' is the effective cohesion; ϕ' is the effective angle of internal friction; $(\sigma - u_a)$ is net normal stress on the failure plane at failure; $(u_a - u_w)$ is the matric suction; σ is the total normal stress; u_a is the pore-air pressure; u_w is the pore-water pressure; χ is a parameter dependent on degree of saturation. The extended Mohr–Coulomb failure envelope is shown in Figure 1.
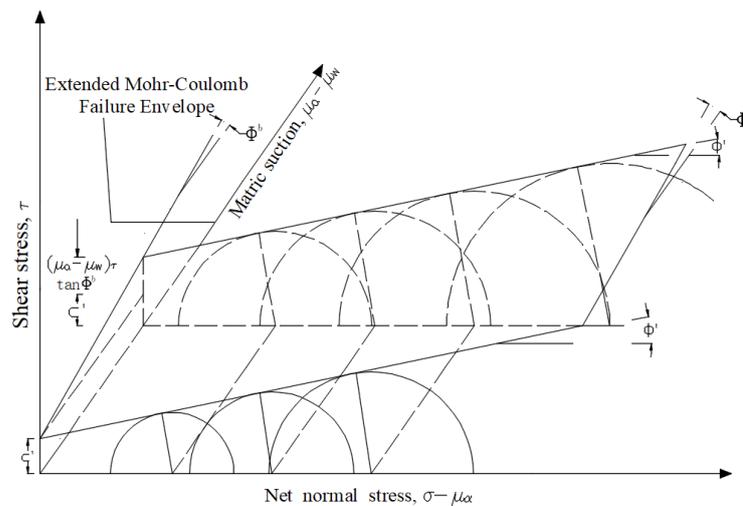
Figure 1. Extended failure linear envelope in the Mohr–Coulomb diagram.

2.2. Van Genuchten SWCC Model

Many models that considered matric suction and the degree of saturation are listed in the literature [16,28,29]. In this study, the vG numerical model was selected because this model has been widely used for various soil types and this model has many advantages such as the documented quality as well as numerical reliability. In the vG numerical model, the relationship between matric suction and the degree of saturation can be expressed as follows:

$$P_c = -P_0 \left[\left(\frac{S_r - S_{rw}}{1 - S_{rw}} \right)^{-1/m} - 1 \right]^{1-m} \tag{2}$$

where P_c is the matric suction; P_0 and m are curve-fitting parameters P_0 is a pressure scaling factor corresponding approximately to the inflexion point of the retention curve; m is a parameter related to the material characteristic; S_r is the degree of saturation; S_{rw} is the residual degree of saturation.

2.3. Khalili Model

To evaluate the relationship between the effective stress parameter χ and the suction, a new equation was proposed by Khalili [22] using Equation (3).

$$\chi = \begin{cases} \left(\frac{u_a - u_w}{u_e} \right)^{-0.55}, & u_a - u_w > u_e \\ 1, & u_a - u_w < u_e \end{cases} \tag{3}$$

where u_e is the matric suction, which means the transition from the state of the saturated zone to unsaturated zone. In Khalili's experiment, the value of u_e was equal to 1 kPa. When $(u_a - u_w) < u_e$, the effective stress parameter χ is 1; when $(u_a - u_w) > u_e$, the effective stress parameter χ decreases with rising matric suction. The effective stress parameter χ ranges from 0 to 1. The right member of Equation (3) can be rewritten as $[u_e / (u_a - u_w)]^{0.55}$. As the suction is located in the position of the denominator, we can infer that the relationship between the effective stress parameter χ and the saturation presents an opposite trend against the soil–water characteristic curve, which has the shape of the letter 'S', and this relationship can be described as the Sigmoid function (logistic function) [30]. Figure 2 shows the SWCC, which was given by van Genuchten [29] and Figure 3 depicts the hypothetical curve that refers to the relationship between the effective stress parameter χ and the degree of saturation. When the saturation approaches 100%, the effective stress parameter χ is close to 1. When the saturation approaches 0%, the effective stress parameter χ is close to 0. The relationship between the effective stress parameter χ and the degree of saturation

is like the letter 'S' (Sigmoid function) and Equation (4) gives the expression of the curve 'S' [31]:

$$\chi = \frac{\xi_1}{1 + \xi_2 e^{\xi_3 S_r}} \tag{4}$$

where ξ_1, ξ_2 and ξ_3 are fitting parameters; e is the Euler's constant (approximately 2.7183).
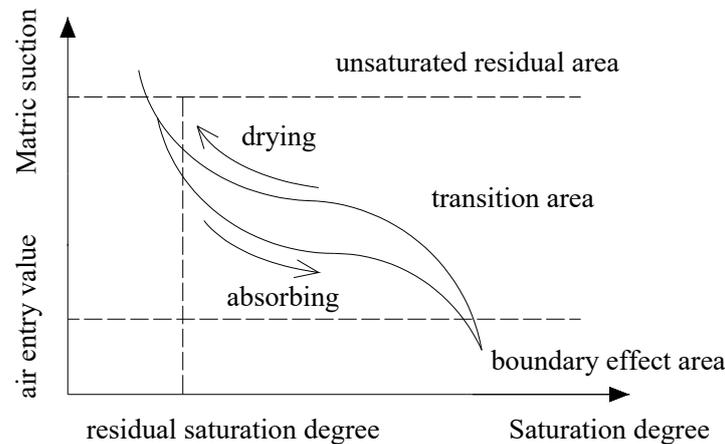

Figure 2. Soil–water characteristic curve.
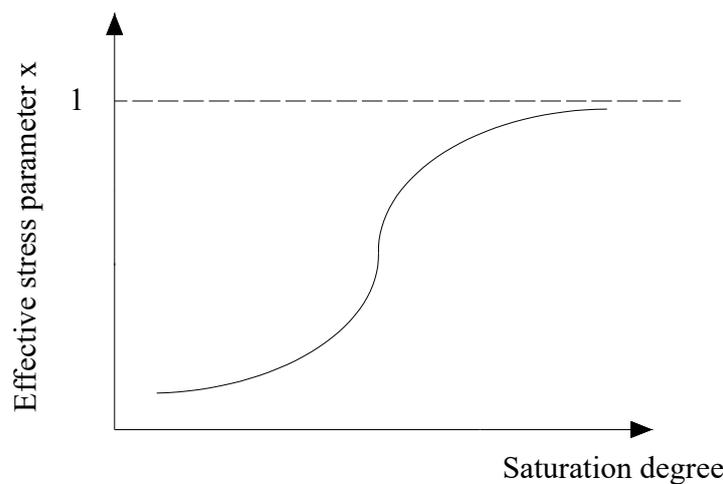
Figure 3. Effect of the saturation degree on the effective stress parameter χ.

2.4. The New Model

Equations (2) and (4) can be put into Equation (1) to obtain the final shear strength model, which includes the degree of saturation, the net normal stress, the effective cohesion, and the internal friction angle. Equation (5) shows the expression of the shear strength model of multiple parameters:

$$\tau_f = c' + \left\{ (\sigma - u_a) + \frac{\xi_4}{1 + \xi_2 e^{\xi_3 S_r}} \cdot [(\frac{S_r - S_{rw}}{1 - S_{rw}})^{-1/m} - 1]^{1-m} \right\} tan\phi' \tag{5}$$

where ξ_2, ξ_3, and ξ_4 are the fitting parameters, ξ_4 is a parameter that is related to air entry value $(\xi_4 = \xi_1 \cdot P_0)$; m is a parameter that is related to the material characteristics; S_r is the degree of saturation; S_{rw} is the residual degree of saturation; c' is the effective cohesion; ϕ' is the effective internal friction angle; $(\sigma - u_a)$ is the net normal stress.

3. Materials and Experimental System

The soil tested in this study was obtained from The Three Gorges region in China. The soil selected was characterized by a clayey fraction (1.88%), silty fraction (14.17%), and sandy fraction (83.95%). Table 1 presents the simple physical properties of the chosen soil. It can be seen that the soil sample can be regarded as silty sand because of its physical properties such as a high water content (ω) and voids ratio (e), a low permeability coefficient (K), a high liquid limit (LL), and a high plastic limit (PL). By adopting sieving and hydrometer methods, the particle-size distribution of this soil was also measured, where the sand particles were the largest.

Table 1. The physical properties of silty sand.

Specific Gravity (G_s)	ω (%)	e	$K \times 10^{-10}$ (m s^{-1})	Particle Composition (%)		
				0.05–2 (mm)	0.002–0.05 (mm)	<0.002 (mm)
2.70	32.5	1.45	1.74	87.8	10.6	1.6

3.1. Soil–Water Characteristic Curve Test

In order to validate the rationality of the formula, we adopted a pressure-plate system to control the suction and define the parameters of the SWCC (vG numerical model). The experimental device is shown in Figure 4, which was made up of a soil sample chamber, pressure control equipment as well as an outflow measurement device [32]. The silty sand was put in the soil specimen chamber. The pressure control equipment controlled air pressure applied to the soil specimen. The outflow measurement device can collect and measure water saturation in order to calculate the variation in the water saturation from the bottom outflow. The silty sand was compacted in a ring (diameter: 70 mm, height: 20 mm) to achieve a dry density of 1.5 t/m^3, 1.6 t/m^3, and 1.7 t/m^3. Before loading, the soil specimens in the rings were saturated with water. After loading, the specimen's soil–water characteristic test at a temperature of 25 °C (normal temperature) was measured using the pressure plate method (Figure 5) or the pressure plate test; the test started with a saturated sample. The degree of saturation was determined by weighing the wet soil sample.
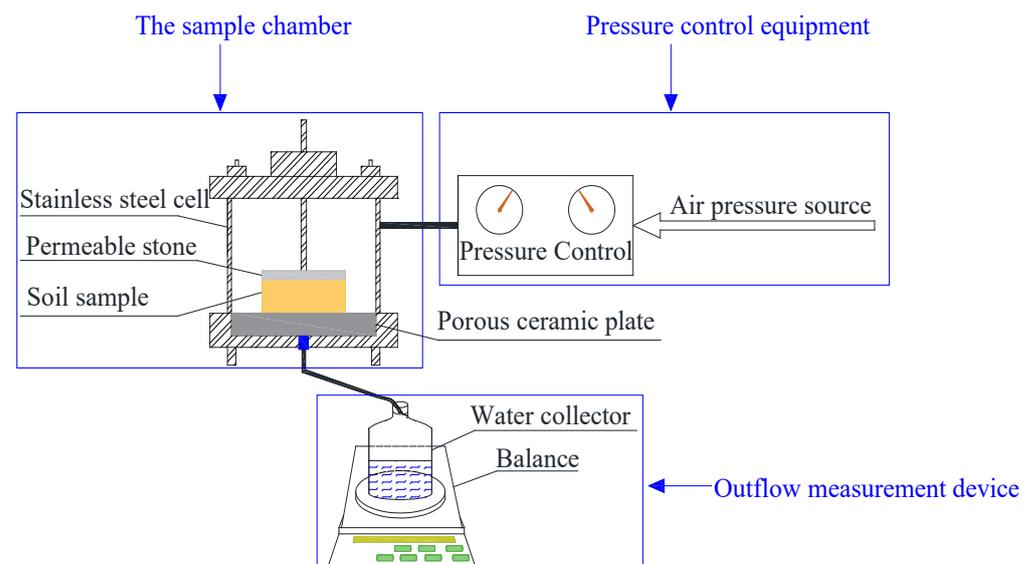

Figure 4. General scheme of the soil–water characteristic curve test system.

Figure 5. Test system of the soil–water characteristic curve using the pressure plate apparatus.

3.2. Shear Strength Test

In order to validate Equation (5), a triaxial shear apparatus (Figure 6) was adopted to control the shear strength and determine the parameters of the proposed model. The silty clay was compacted in a triaxial saturator (diameter: 61.2 mm, height: 125 mm). After taking apart the triaxial saturator, the soil enclosed with a rubber membrane was put into the triaxial compression apparatus (Figure 7), then many triaxial compression tests with various degrees of saturation (30%, 40%, 50%, 60%, 70%, 80%, 90%) under different confining pressures including 50 kPa, 100 kPa, 150 kPa, and 200 kPa were conducted. The initial confining pressure for the triaxial shear test was often set at a low value such as 50 kPa to ensure that the sample was not damaged during the initial stages of the test. The reason why the effective confining pressure was set at a low value was that the soil sample had relatively low strength, and this sample can be adequately tested by lower confining pressures. Excessive pressure could cause damage to the sample, which could result in inaccurate results. In addition, the sample may experience excessive deformation, failure, or crushing at higher pressures, which could also affect the shear strength parameters. The mass of the soil sample and the mass of water need to be measured in advance to put them together so that the degree of saturation is determined. Degree of saturation = (mass of water added/(mass of solid + mass of water added)) × 100%.
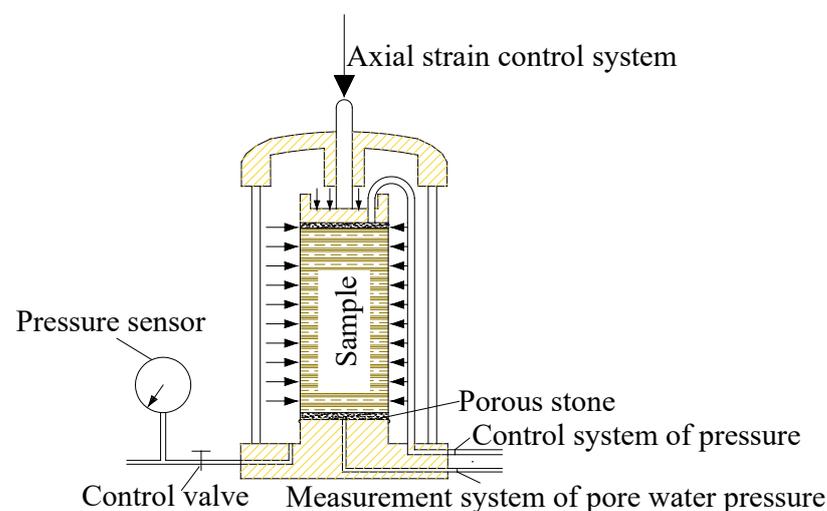

Figure 6. General scheme of the triaxial shear test system.

Figure 7. Test system of the triaxial shear apparatus.

Moreover, the shearing velocity was 0.2 mm/min. There are three types of triaxial shear test including a consolidated drained triaxial test (CD test), a consolidation undrained test (CU test), and an undrained and unconsolidated test (UU test). In this study, the consolidated drained triaxial test (CD test) was conducted on saturated soil, and the consolidation undrained test was conducted on unsaturated soil. In this research, the CU test was adopted as the experiment aimed for unsaturated soil.

4. Results and Discussion

4.1. Comparison with Experimental Data

For the curve fitting, the nonlinear least squares method was applied to get the parameters of the vG numerical model and the Equation (4). Table 2 lists four parameters that were calculated under three various dry densities ($\rho_d = 1.5$ t/m^3, $\rho_d = 1.6$ t/m^3, $\rho_d = 1.7$ t/m^3).

Table 2. Values of the model parameter fitting for the experimental points.

Parameter	ξ_2	ξ_3	$\xi_4 = \xi_1 \cdot P_0$	m
$\rho_d = 1.5$ t/m^3	40,009.57	−4.21	20,295.99	0.24
$\rho_d = 1.6$ t/m^3	40,017.51	−4.51	11,675.79	0.21
$\rho_d = 1.7$ t/m^3	64,735.01	−5.01	9886.80	0.20

The soil–water characteristic curve of the soil measured at various dry densities and fitted curve is plotted in Figure 8. As shown in Figure 8, the predicted curve provided good consistency with the experimental points because the correlation coefficient was 0.95. This also verified the vG numerical model. For a rising degree of saturation, the matric suction declined. Further analysis revealed that when the degree of saturation was less than 50%, the suction rose with increasing dry density. When the soil became increasingly compacted, the voids became smaller and the bonding situation of the soil particles became increasingly tight. This is why matric suction decreased with an increasing degree of saturation. There was no significant variation in the matric suction when the saturation was more than 50%. In the boundary effect stage, as the number of large pores containing free water reduces with increasing dry density, the declining amplitude of the volumetric water content decreases with the increasing matric suction. In the transition stage, the higher the dry density of silty sand, the greater the air entry value of the sample. It is really difficult for soil samples of higher dry density to evolve from a saturated state to an

unsaturated state. The larger dry density corresponds to the larger pores with free water, fewer pores as well as poorer connectivity of water, as a result, it is difficult for water to drain out of the sample. Therefore, if the sample wanted to evolve from the quasi-saturated status to unsaturated status, it would need more matric suction. In the residual stage, the residual volumetric water content of the sample increased with increasing dry density. There were more soil particles in the samples with higher dry density, which could provide more adsorption space (such as pores on the surface of particles and small pores between particles) for capillary water and bound water.
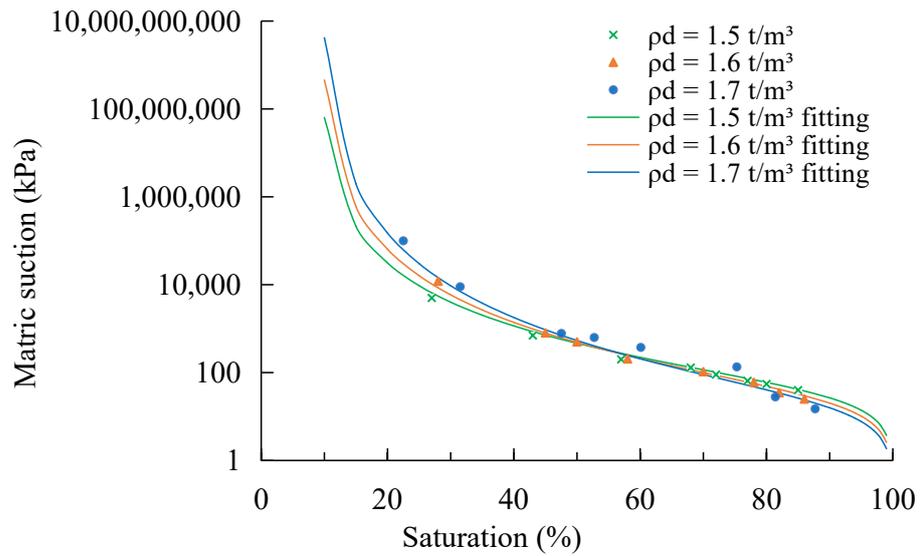
Figure 8. SWCC based on the experimental points and fitted curve at various dry densities.

Figure 9 shows that the effective stress parameter of the unsaturated soil increased with a rising degree of saturation and the shape of this curve looked like the letter 'S'. The correlation coefficient between the modeled and experimental data was 0.98, which can also be regarded as a validation of Equation (4).
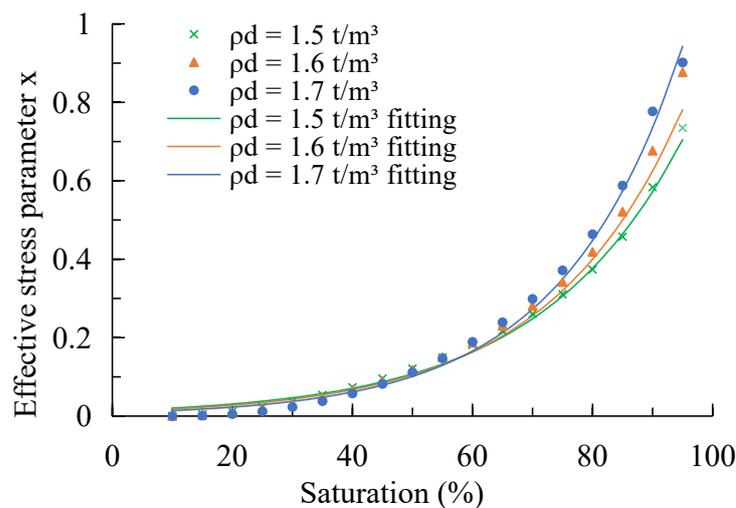
Figure 9. The effective stress parameter χ of the calculated points and fitted curve at various dry densities.

The relationship between the principal stress difference and axial strain was plotted with the principal stress difference as the vertical axis and axial strain as the horizontal

axis (Figure 10a). As outlined in the Chinese Standards for Soil Test Methods (GB/T50123-1999), the test should be stopped when the total axial strain is 20%. If there is no peak, we considered a shear peak at 15% of the axial strain as the principal stress difference of the soil sample. Then, a failure shear stress circle was plotted, with the shear stress as the vertical axis and normal stress as the horizontal axis, which can be obtained to calculate the shear strength parameters (Figure 10b). In the plot, the circles were around $(\sigma_1 + \sigma_3)/2$ with a radius of $(\sigma_1 - \sigma_3)/2$ at failure.
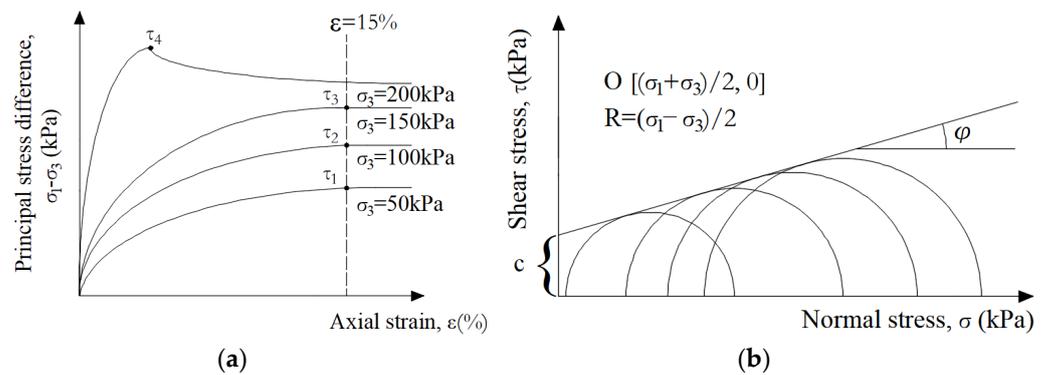
Figure 10. The schematic diagram of the soil shear strength parameter calculation. (**a**) Stress–strain curve. (**b**) Mohr's circle.

For this experiment, a total of 84 tests carried out with four different confining pressures, three different dry densities, and seven different initial saturations ($4 \times 3 \times 7$). Hence, 84 circles were displayed in the final diagram. Then, the cohesion and angle of friction were obtained by measuring the intercept and slope of the failure envelope. The stress–strain curve of the soil with the dry density of 1.6 t/m^3 and the confining pressure of 150 kPa under the saturation of 30%, 40%, 50%, 60%, and 70% is shown in Figure 11. The curve with a saturation of 70% and confining pressure of 150 kPa under the dry density of 1.5 t/m^3, 1.6 t/m^3, and 1.7 t/m^3 is plotted in Figure 12. If the specimen is made up of saturated soil, the shear strength is constant under different cell pressures. Consequently, the failure envelope will be parallel to the horizontal axis because the angle of friction is zero. The other situation is that if the specimen is not saturated, the shear strength will increase as the confining pressure increases. When the result was plotted, it can be seen that the size of the circles increased and the failure envelope was an inclined line.
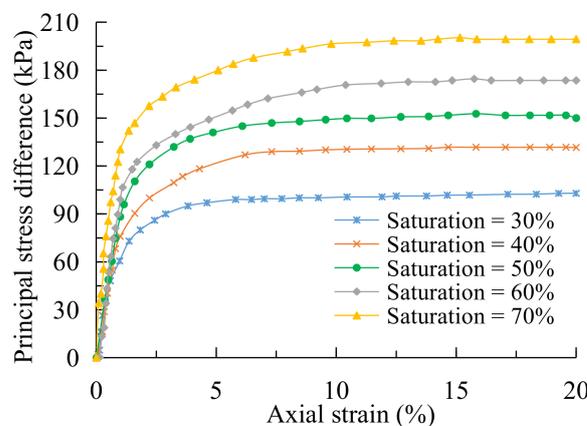

Figure 11. Stress–strain curve under various saturations (ρ_d = 1.6 t/m^3, $\sigma - \mu_a$ = 150 kPa).
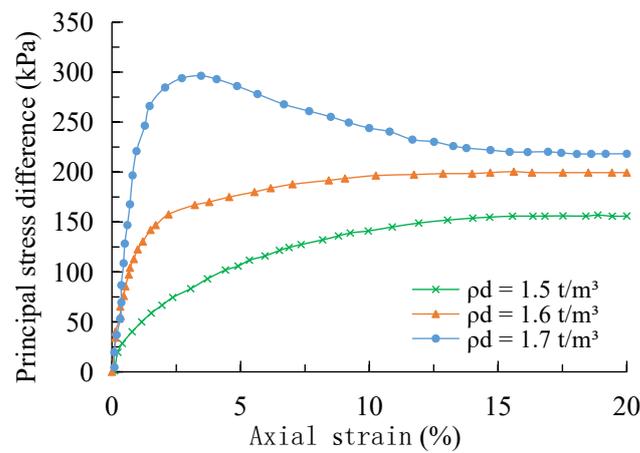
Figure 12. Stress–strain curve under various dry densities (Saturation = 70%, $\sigma - \mu_a$ = 150 kPa).

Figure 13 shows the relation between cohesion and saturation. There was a peak of cohesion at various dry densities when using the traditional test method of compaction. When the saturation was less than 40%, the cohesion showed an upward trend with an increasing degree of saturation, because a remolded soil sample made by dry soil and water was compacted in layers. The absorption between the soil layer and particles is weak and it is easy for a soil sample to be broken, especially in the link between two layers. When the saturation degree increases, the absorption between the soil layer and particles increases, so the cohesion increases. When the saturation is more than 40%, the thickness of the mucosa between the soil particles increases, the effective stress declines as a result, and the cohesion showed a downward trend. In addition, when the dry density increased, the distance between the soil particles became smaller, the absorption became stronger, and the cohesion became stronger.
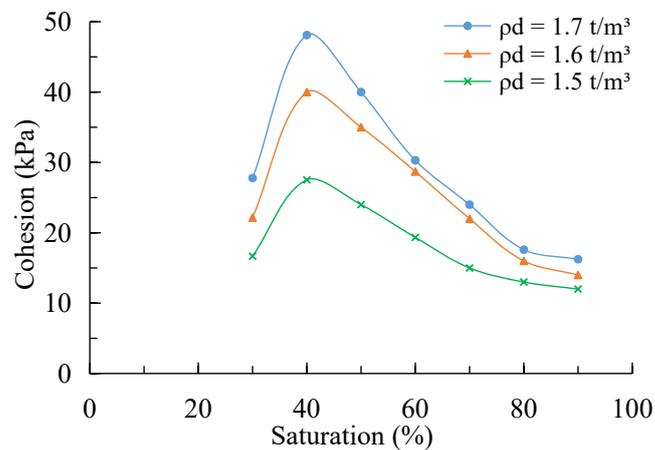
Figure 13. Experiment points of the relationship between cohesion and saturation.

Figure 14 shows that the internal friction angle declined with climbing saturation. It is generally acknowledged that the total internal friction is made up of sliding friction, which is related to the mineral composition of the soil, the friction caused by dilatancy as well as friction caused by broken particles or the rearrangement of particles. When the water content increases gradually, the combined water film around the soil particles thickens; as a result, the amount of free water increases, then lubrication increases, and the friction between soil particles declines. This is why the internal friction angle showed a downward trend. In addition, when the dry density increased, the original structure became tighter. Then, the friction increased, which led to an increase in the internal friction angle.
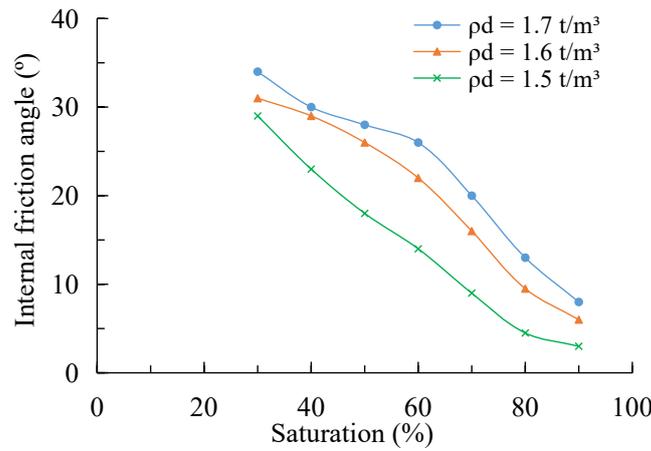
Figure 14. Experimental points of the relationship between the internal friction angle and saturation.

Figure 15 shows that shear strength dropped gradually with the degree of saturation. Measured values of the shear strength at higher dry density were greater than those measured in specimens with a lower dry density. The relationship between shear strength and degree of saturation at various net normal stresses is shown in Figure 16. As the net normal stress ($\sigma - \mu_a$) became higher, the shear strength became higher.
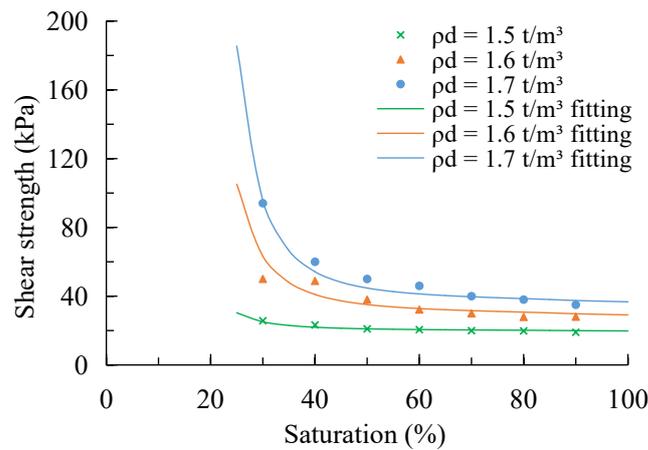
Figure 15. Experimental points and fitted curve of the shear strength at various dry densities.
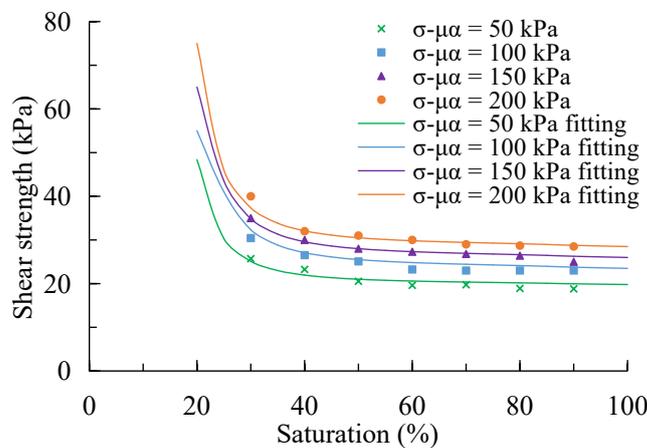
Figure 16. Experimental points and fitted curve of the shear strength at various net normal stresses.

The measured results and the calculated values for shear strength by the proposed model are compared in Figure 17. The difference between the experimental and calculated results was generally less than 7%, indicating that the calculated shear strength using the proposed model agreed well with the measured shear strength. The comparison of this result therefore confirms the reliability of the proposed model.
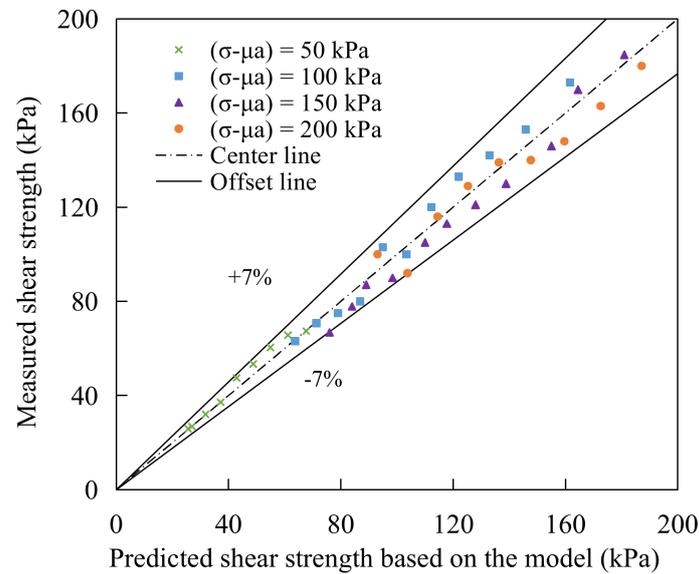

Figure 17. The comparison between the predicted and measured shear strength.

4.2. Comparison with Literature Data from Clayed-Silty Sand and Ankara Clay

In order to further examine the predictive values of Equation (5), we refer to the laboratory test reported in Tomoyoshi [26] and Erdal [27] in the case of the clayed-silty sand and Ankara clay, respectively. The four optimal parameters in Equation (5) proposed in this paper were also computed by employing the nonlinear least squares method (Table 3).

Table 3. Values of the model parameter fitting for the literature data.

Parameter	ξ_2	ξ_3	$\xi_4 = \xi_1 \cdot P_0$	m
Clayed-silty sand (e = 1.31)	2.63	−1.42	6.52	0.82
Clayed-silty sand (e = 1.08)	89.07	−1.79	551.05	0.58
Ankara clay	52.59	−3.42	160.82	0.38

Clayed-Silty sand. The clayed-silty sand (sand 0%, silt 92%, clay 8%) has a relatively uniform grain-size distribution with a median grain size D50 of approximately 0.1 mm. Tomoyoshi [26] also adopted a pressure-plate system to test the soil–water characteristic curve, a method similar to this research. The difference was that he used the direct shear apparatus to obtain the shear strength. The relationship between matric suction, effective stress parameter, and saturation of various compaction pressures for the modeled data and measured data are presented in Figures 18 and 19, respectively. Figures 20 and 21 show the prediction of the proposed model for the clayed-silty sand for various compaction pressures. The computed results were compared with the reported data in that study. The correlation coefficients between the experimental data and fitting data were 0.95 and 0.98 at a compaction pressure of 100 kPa and 600 kPa, respectively.
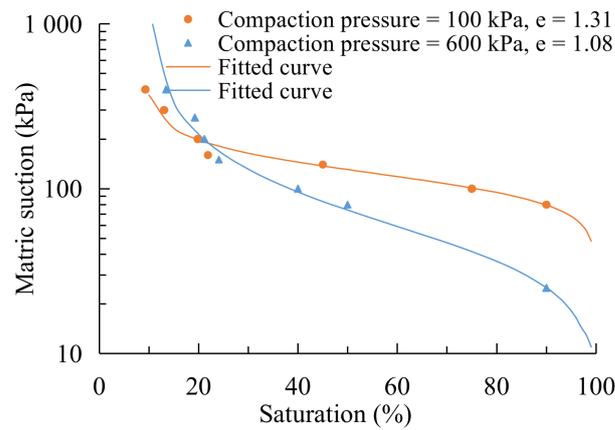
Figure 18. Soil–water characteristic curve of the experimental points and fitted curve at different compaction pressures.
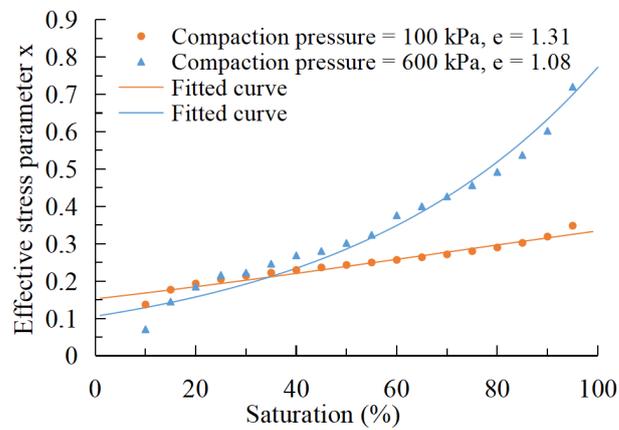

Figure 19. Effective stress parameter χ of the calculated points and fitted curve at different compaction pressures.
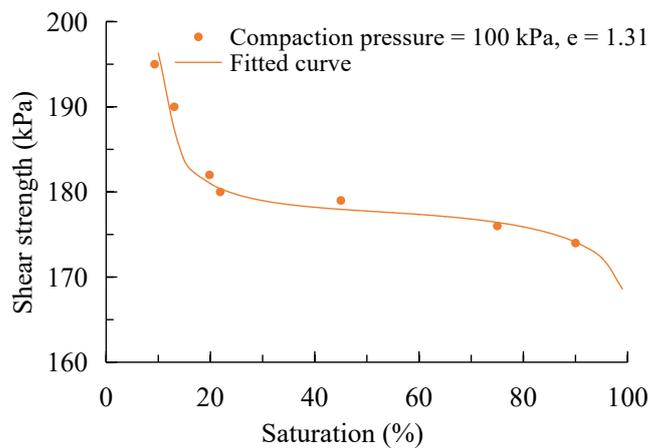

Figure 20. Calculated results on the shear strength of the compaction pressure for 100 kPa.
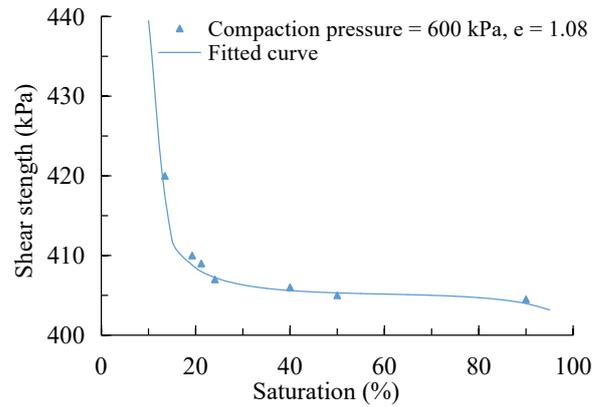
Figure 21. Calculated results on the shear strength of the compaction pressure for 600 kPa.

Clayey soil. The clayey soil (clay fraction 67.9%) researched by Erdal [27] was obtained from METU (Middle East Technical University). The specific gravity was 2.73, the liquid limit was 48%, the plastic limit was 21%, and the plasticity index was 27%. Figures 22 and 23 show the modeled and experimental data for the relationship between matric suction and saturation as well as the effective stress parameter, respectively, with good agreement. The relationship between the shear strength and saturation under various net normal stresses is shown in Figure 24. The calculated values were close to the experimental points in Erdal's paper. All correlation coefficients were larger than 0.98.
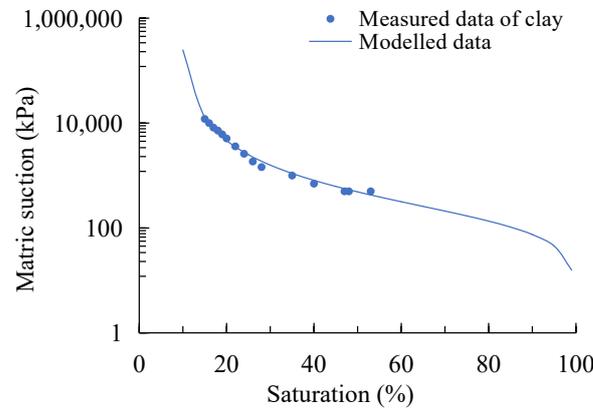

Figure 22. Soil–water characteristic curve based on experimental points [27] and the fitted curve.
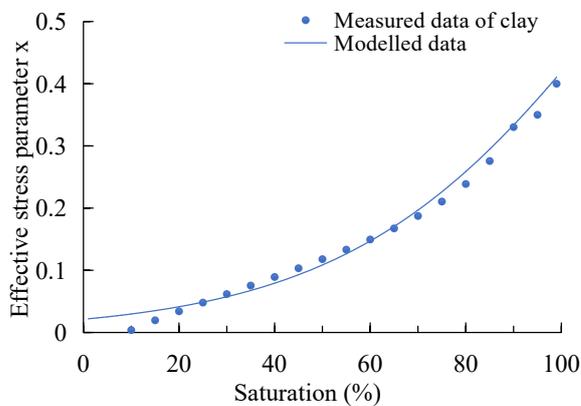

Figure 23. Effective stress parameter χ based on the calculated data [27] and the fitted curve.
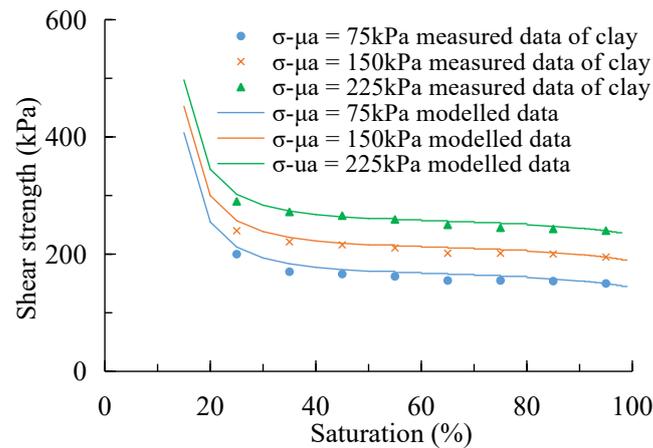
Figure 24. Comparison of the calculated shear strength of the proposed model and the experimental data [27].

In geotechnical engineering, after obtaining the soil sample using a cutting ring, it is easy for engineers to obtain the degree of saturation through a simple laboratory test. The measurement of the matric suction is expensive, time-consuming, and difficult. Therefore, knowing the degree of saturation, the shear strength can be determined using Equation (5) without knowledge of the matric suction. This could also guide practical engineering applications such as slope stability.

5. Sensitivity Analysis of Four Parameters

The parameter sensitivity analysis was conducted to examine the robustness of the proposed model and evaluate whether varying key parameters affected the results. In this model calculation, one parameter was changed while the others remained fixed at their optimal value. The result of the parameter sensitivity analysis is shown in Figure 25. Take $\rho_d = 1.5$ t/m^3 as an example, the ranges of four parameters are shown as follows: ξ_2, [38912.99, 41929.02]; ξ_3, [−4.184, −4.049]; ξ_4, [19883.32, 20763.47]; m, [0.2397, 0.2429]. By comparing the range of shear strength under the variation of the one parameter, we found that this model was much more sensitive regarding the parameter m, which is also related to the material characteristic. When soil is close to a saturated status, the shear strength tends to a stable value. This is because the softening effect of soil against shear strength is much more obvious when soil tends to the saturated status.


Sensitivity of ξ_2
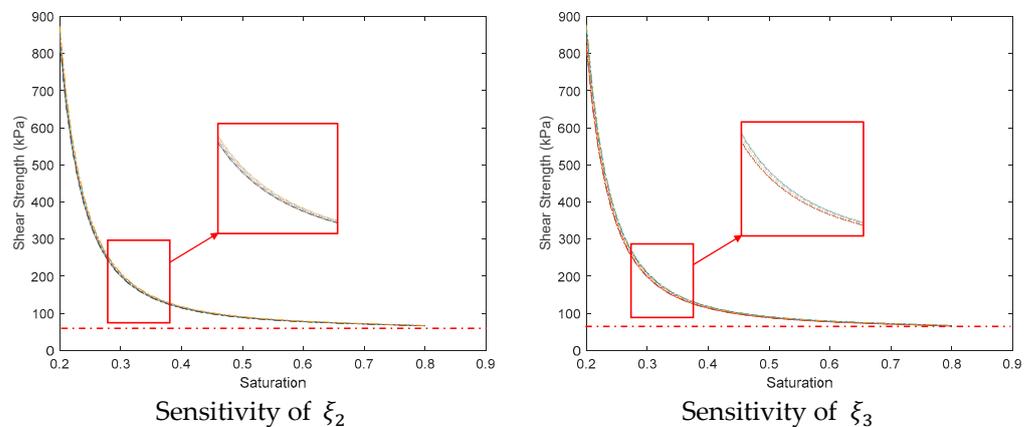
Sensitivity of ξ_3
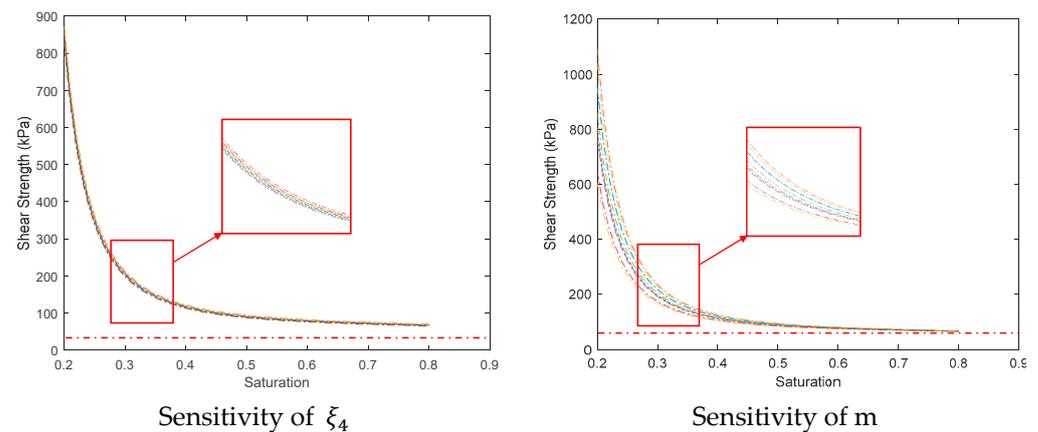
Figure 25. *Cont.*

Figure 25. Comparison for sensitivity of the four parameters.

6. Conclusions

In geotechnical engineering, the measurement of saturation degree is relatively simple through laboratory tests, however, the measurement of matric suction is expensive, time-consuming, and difficult. Therefore, in this paper, a new shear strength model was developed, applied, and tested for applications in engineering problems related to unsaturated soil. Test results indicate that this model is of good quality to be used in engineering to predict the relationship between the degree of saturation and shear strength with a wide range of soils.

The new shear strength model describing the degree of saturation is expressed as a multiple parameter equation. Based on Bishop's shear strength theory and the van Genuchten model for the soil–water characteristic curve, the proposed model can be expressed as a function of saturation, residual degree of saturation, effective shear strength indices (effective cohesion and internal friction angle), net normal stress, and five characterization parameters (ξ_2, ξ_3, ξ_4, m, S_{rw}); S_{rw} is the residual saturation, ξ_2 and ξ_3 are fitting parameters, ξ_4 is related to the air entry value $\left(\xi_4 = \xi_1 \cdot P_0\right)$, and m is related to the material characteristic. In addition, the expression of the effective stress parameter is described as a Sigmoid function. Comparing the result of shear strength under the variation of one parameter, we found that this model was much more sensitive regarding the parameter m, which is related to the material characteristic.

The validation of this proposed model was based on laboratory tests for the determination of the soil–water characteristic curve and the triaxial shear strength tests of silty sand. The predicted results were close to the experimental points and the maximum discrepancy was less than 7%. Furthermore, the calculated results acquired from the proposed model were compared with the experimental points of the previously published data including the clayed-silty sand and Ankara clay. The comparison between the theoretical prediction and experimental points is promising; this also shows the adaptability of the proposed model to a wide range of soils.

This model can also be incorporated into analytical solutions and the numerical simulation of slope stability in unsaturated soils. The degree of saturation can be considered in the unsaturated soil shear strength directly and shear strength can be predicted by using a simple method to test the degree of saturation after obtaining the soil sample by using a cutting ring to avoid the complex measurement of the matric suction. Therefore, knowing the degree of saturation, the shear strength can be determined using Equation (5) without the knowledge of the matric suction. This could also give guidance to practical engineering applications such as slope stability. Simultaneously, there are further effects to be added, and a multiple parameter and complex coupling model that considers temperature will be explored in the immediate future.

References

1.　Cho, S.E. Stability analysis of unsaturated soil slopes considering water-air flow caused by rainfall infiltration. *Eng. Geol.* **2016**, *211*, 184–197. [CrossRef]

2.　Hu, R.; Chen, Y.; Zhou, C. Modeling of coupled deformation, water flow and gas transport in soil slopes subjected to rain infiltration. *Sci. China Technol. Sci.* **2011**, *54*, 2561. [CrossRef]

3.　Xu, W.J.; Wang, Y.J.; Dong, X.Y. Influence of reservoir water level variations on slope stability and evaluation of landslide tsunami. *Bull. Eng. Geol. Environ.* **2021**, *80*, 4891–4907. [CrossRef]

4.　Liu, G.; Tong, F.; Tian, B. Influence of atmospheric temperature on shallow slope stability. *Environ. Earth Sci.* **2019**, *78*, 632. [CrossRef]

5.　Chen, G.; Meng, X.; Qiao, L. Response of a loess landslide to rainfall: Observations from a field artificial rainfall experiment in Bailong River Basin, China. *Landslides* **2018**, *15*, 895–911. [CrossRef]

6.　Hou, X.; Li, T.; Qi, S. Investigation of the cumulative influence of infiltration on the slope stability with a thick unsaturated zone. *Bull. Eng. Geol. Environ.* **2021**, *80*, 5467–5480. [CrossRef]

7.　Nguyen, T.S.; Likitlersuang, S. Reliability analysis of unsaturated soil slope stability under infiltration considering hydraulic and shear strength parameters. *Bull. Eng. Geol. Environ.* **2019**, *78*, 5727–5743. [CrossRef]

8.　Dou, H.Q.; Han, T.C.; Gong, X.N. Effects of the spatial variability of permeability on rainfall-induced landslides. *Eng. Geol.* **2015**, *192*, 92–100. [CrossRef]

9.　Li, B.; Tian, B.; Tong, F.G.; Liu, C. Effect of the Water-Air Coupling on the Stability of Rainfall-Induced Landslides Using a Coupled Infiltration and Hydromechanical Model. *Geofluids* **2022**, *2022*, 3036905. [CrossRef]

10.　Vanapalli, S.K.; Fredlund, D.G. Comparison of different procedures to predict unsaturated soil shear strength. In *Advances in Unsaturated Geotechnics*; Geotechnical Special Publication; American Society of Civil Engineers: Reston, VA, USA, 2000; pp. 195–209.

11.　Bishop, A.W. The principle of effective stress. Lecture delivered in Oslo. *Tek. Ukebl.* **1959**, *39*, 859–863.

12.　Bishop, A.W.; Alpan, I.; Blight, G.E.; Donald, I.B. Factors controlling the shear strength of partly saturated cohesive soils. In Proceedings of the 5th International Conference on Soil Mechanics Foundation Engineering, Paris, France, 17–22 July 1961.

13.　Bishop, A.W. The measurement of pore pressure in the triaxial test. Pore Pressure and Suction in Soils. In Proceedings of the Conference on Pore Pressure and Suction in Soils, London, UK, 30–31 March 1960.

14.　Fredlund, D.G.; Morgenstern, N.R.; Widger, R.A. The shear strength of unsaturated soils. *Can. Geotech. J.* **1978**, *15*, 313–321. [CrossRef]

15.　Fredlund, D.G.; Rahardjo, H. *Soil Mechanics for Unsaturated Soils*; John Wiley and Sons, Inc.: New York, NY, USA, 1993.

16.　Fredlund, D.G.; Xing, A.; Fredlund, M.D.; Barbour, S.L. Relationship of the unsaturated soil shear strength to the soil-water characteristic curve. *Can. Geotech. J.* **1996**, *33*, 440–448. [CrossRef]

17.　Abramento, C. Geotechnical parameters for the study of natural slopes instabiliza tion at 'Serra do Mar', Brazil. In Proceedings of the 12th International Conference on Soil Mechanics and Foundation Engineering, Rio De Janeiro, Brazil, 13–18 August 1989.

18.　Toll, D.G. A framework for unsaturated soils behavior. *Géotechnique* **1990**, *40*, 31–44. [CrossRef]

19.　Öberg, A.L.; Sällfors, G. Determination of Shear Strength Parameters of Unsaturated Silts and Sands Based on the Water Retention Curve. *Geotech. Test. J.* **1997**, *20*, 40–48. [CrossRef]

20.　Zhang, C.; Lu, N. Unified effective stress equation for soil. *J. Eng. Mech.* **2020**, *146*, 04019135. [CrossRef]

21.　Lu, N.; Godt, J.W.; Wu, D.T. A closed-form equation for effective stress in unsaturated soil. *Water Resour. Res.* **2020**, *46*, W05515. [CrossRef]

22.　Khalili, N.; Khabbaz, M.H. A unique relationship for χ for the determination of the shear strength of unsaturated soils. *Géotechnique* **1998**, *48*, 681–687. [CrossRef]

23. Jiang, M.J.; Leroueil, S.; Konrad, J.M. Insight into shear strength functions of unsaturated granulates by DEM analyses. *Comput. Geotech.* **2004**, *31*, 473–489. [CrossRef]

24. Tong, F.; Jing, L.; Bin, T. A Water Retention Curve Model for the Simulation of Coupled Thermo-Hydro-Mechanical Processes in Geological Porous Media. *Transp. Porous Media* **2012**, *91*, 509–530. [CrossRef]

25. Abdulrahman, A.; Marwen, B.; Muzahim, A. Effect of long-term soaking and leaching on the behavior of lime-stabilized gypseous soil. *Int. J. Pavement Eng.* **2015**, *16*, 11–26. [CrossRef]

26. Tomoyoshi, N.; Yasunari, H.; Fredlund, D.G.; Gan, J.K. Influence of stress history on the strength parameters of an unsaturated statically compacted soil. *Can. Geotech. J.* **1999**, *36*, 251–261. [CrossRef]

27. Erdal, C.; Hüseyin, P.T. Shear strength-suction relationship of compacted Ankara clay. *Appl. Clay Sci.* **2010**, *49*, 400–404. [CrossRef]

28. Brooks, R.J.; Corey, A.T. Hydraulic Properties of Porous Media. Ph.D. Thesis, Colorado State University, Fort Collins, CO, USA, 1965.

29. Van Genuchten, M.T. A closed-form equation for predicting the hydraulic conductivity of unsaturated soils. *Soil Sci. Soc. Am.* **1980**, *44*, 898. [CrossRef]

30. Bisong, E. Logistic Regression. In *Building Machine Learning and Deep Learning Models on Google Cloud Platform*; Apress: Berkeley, CA, USA, 2019. [CrossRef]

31. Kim, D.N.; Chen, I.M.; Teck, C.N. Planning algorithms for s-curve trajectories. In Proceedings of the IEEE/ASME International Conference on Advanced Intelligent Mechatronics, Zurich, Switzerland, 4–7 September 2007.

32. Liu, C.; Li, B.; Tong, F. Determination of soil-water retention curve from a transient air-water two-phase outflow experiment. *Bull. Eng. Geol. Environ.* **2020**, *79*, 2109–2118. [CrossRef]